THE JOURNAL OF PHYSICAL CHEMISTRY C

Article

pubs.acs.org/JPCC

Structural and Optoelectronic Properties of Unsaturated ZnO and ZnS Nanoclusters

Giuliano Malloci,*[,†] Letizia Chiodo,[‡] Angel Rubio,[§] and Alessandro Mattoni*[,†]

[†]Istituto Officina dei Materiali (CNRIOM), Unità di Cagliari, Cittadella Universitaria, I-09042 Monserrato (Ca), Italy

[‡]Center for Biomolecular Nanotechnologies @UNILE, Istituto Italiano di Tecnologia, and European Theoretical Spectroscopy Facility, Via Barsanti, I-73010 Arnesano, Italy

[§]European Theoretical Spectroscopy Facility (ETSF), and Nano-Bio Spectroscopy Group, ETSF Scientific Development Centre, Universidad del País Vasco, CFM-CSIC-UPV/EHU-MPC and DIPC, Avenida Tolosa 72, E-20018 San Sebastián, Spain

Supporting Information

ABSTRACT: We report a systematic computational study of the structural and optoelectronic properties of unsaturated ZnO and ZnS nanoclusters with hexagonal prism structure, as a function of length and diameter. We computed the fundamental gap using density functional theory (DFT) in the framework of the ΔSCF scheme and the optical gap by means of time-dependent DFT (TDDFT). We found that all ZnO nanostructures transform from wurtzite to graphitic phase. On the contrary, ZnS nanocrystals with diameters above ∼1 nm are found to transform to a zeolite BCT phase. These different structural properties reflect in a very different size dependence of the electronic and optical properties, with a strong discontinuity for ZnS particles. The correlation between morphology and optoelectronic properties is demonstrated by considering models of saturated clusters preserving the wurtzite phase. We additionally compared DFT/TDDFT results with many-body perturbation theory methods showing a general good agreement among the two techniques for this class of nanocrystals of the two materials.

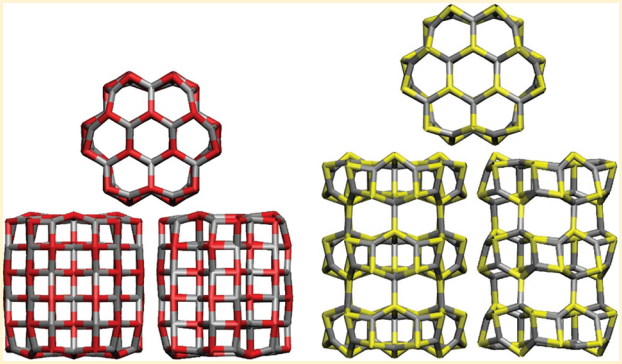

1. INTRODUCTION

Since the discovery of fullerenes[1] and carbon nanotubes,[2] the search for new nanoscaled materials based on elements other than carbon has received much attention. II−VI semiconductors attract intense interest in both nanoscale science and nanotechnology because of their unique electronic and optical properties. Zinc oxide (ZnO) and zinc sulphide (ZnS), in particular, are probably the most studied materials in the II−VI family owing to their high abundance and stability, high transparency, large exciton binding energy, piezoelectricity, and biocompatibility.[3]

ZnO and ZnS share two types of crystal structures: hexagonal wurtzite and cubic zinc blende. Under ambient conditions, ZnO crystallizes in wurtzite form, whereas the most stable polymorph of ZnS is zinc blende. A large variety of ZnO and ZnS nanostructures with different morphologies (rods, wires, tubes, belts, ribbons, sheets, etc.),[4−10] as well as ZnO-ZnS heterostructures,[11,12] have been synthesized. These nanoscaled materials have emerged as promising candidates in a wide number of applications, ranging from optoelectronics and gas-sensing to catalysis and photovoltaics. In the field of photovoltaic energy production, in particular, ZnO is considered to be a good alternative to TiO_2, in both dye-sensitized[13−16] and quantum-dot sensitized[17−19] exciton solar cells.

On the nanoscale, because of the reduced sizes of the particles, new phenomena that are not present in the bulk phase become important. Quantum confinement, for example, gives rise to a size dependence of the electronic and optical properties; in particular, the energy gap increases as the size decreases. At the same time, as a consequence of the large surface/volume ratio, surface effects come into play: atoms on the surface have dangling bonds and tend to rearrange their position. The associated surface energy may favor a particular crystalline structure over another, but the energy balance is, however, strongly dependent on the synthesis conditions (temperature, solvent, saturation, etc.).

Over the years, along with the remarkable amount of experimental work, a large number of theoretical studies devoted to ZnO[20−35] and ZnS[36−49] clusters have been published. These studies have greatly contributed to our knowledge of the structural properties of nanosized ZnO and ZnS particles. For example, ZnO nanostructures are known to transform from wurtzite to graphitic phase below specific critical dimensions.[24,50,51] For the medium-sized clusters (number of dimers n in the range 10−50), hollow structures

Received: October 11, 2011
Revised: March 27, 2012
Published: March 28, 2012

dx.doi.org/10.1021/jp209756z | J. Phys. Chem. C 2012, 116, 8741−8746

with cage and tube-like configuration are found to be the preferred motif, whereas onion-like and wurtzite-like structures become more and more favorable with increasing size.[28,30] For large ZnS clusters, a crystalline phase characterized by the presence of four and six rings has been theoretically predicted by using classical model potentials.[41,45,46] This crystalline phase, analogous to the zeolite structure BCT, has not yet been confirmed experimentally, and the electronic and optical properties of BCT particles are largely unknown to date.

Because of computational limitations, elucidating the electronic and optical properties of realistic $(ZnX)_n$ (X = O,S) nanoparticles with sizes comparable to the experiments is a difficult task. Recent computational work reported models of prismatic $(ZnX)_n$ nanostructures with n = 111 and size ∼1.5 nm.[49] These particle models have been obtained by starting from the bulk wurtzite structure and by saturating the polar Zn- and X-terminated surfaces.

In this Article, we contribute to the modeling of $(ZnX)_n$ nanostructures by performing a systematic comparative study of the structural and optoelectronic properties of unsaturated nanoclusters with hexagonal prism structure as a function of length and diameter. Ground-state structural relaxations performed in the framework of all-electrons density functional theory (DFT)[52] were complemented by the evaluation of the fundamental energy gap in the so-called ΔSCF scheme[53] and the optical gap by means of time-dependent DFT (TDDFT).[54] For all unsaturated clusters, as expected, we found that surface effects give rise to significant structural rearrangements so as to enhance bonding and minimize the net dipole of the system. In particular, after geometry optimization, all unsaturated ZnO nanostructures are found to transform to a graphitic phase, in agreement with previous computational studies.[24,50,51] In the case of ZnS, on the contrary, for diameters above ≃1 nm, we observe a structural transformation to the zeolite BCT phase predicted for large ZnS particles.[41,45,46] The correlation between morphology and optoelectronic properties is demonstrated by considering additional models of saturated clusters preserving the wurtzite phase.[49] From the methodological side, we additionally presented a comparison between DFT/TDDFT and many-body theories showing for both materials a general good agreement between the two techniques for this class of nanocrystals.

2. COMPUTATIONAL DETAILS

DFT calculations have been performed by using the quantum chemistry program package TURBOMOLE. We used the gradient-corrected BP86 exchange-correlation functional[55,56] in conjunction with a TZVP basis set. Additional details of the calculations can be found in the Supporting Information.

The $(ZnO)_n$ nanocrystals were cut out from a bulk wurtzite crystal (a = 3.258 Å, c = 5.220 Å, u = 0.382 Å[57]) and fully relaxed in vacuo. $(ZnS)_n$ nanocrystals were relaxed by starting from the geometry of the corresponding optimized $(ZnO)_n$ clusters. We then used the ΔSCF scheme[52] by evaluating total-energy differences between the self-consistent field calculations performed for the neutral and charged systems (±1) to obtain the vertical electron affinity (EA_v) and the first ionization energy (IE_v). This enabled the calculation of the fundamental gap, which is rigorously defined within the ΔSCF scheme[52] as

$$E_{gap} = IE_v - EA_v = E_{N+1} + E_{N-1} - 2E_N \quad (1)$$

where E_N is the total energy of the N-electron system.

Optical excited states are properly described for finite systems by time-dependent DFT (TDDFT).[54] To compute the excitation energies and electronic absorption spectra, we used two different approaches within TDDFT in conjunction with different representations of the wave functions: (i) the frequency-space implementation[58] based on the linear combination of localized orbitals, which is limited to the low-energy part of the spectrum, and (ii) the real-time propagation scheme using a grid in real space,[59] yielding the complete absorption spectrum. For (i) and (ii) calculations, we used the TURBOMOLE[60] and OCTOPUS packages,[61] respectively. The difference between the fundamental gap computed via eq 1 and the optical gap given by TDDFT enabled a rough estimate of the excitonic effects occurring in these systems.

For the smallest clusters, we additionally made use of many-body perturbation theory (MBPT) to validate the above computational methodology. More specifically, we computed the GW electronic gap within Hedin's GW approximation[53,62,63] and the optical absorption by directly solving the Bethe Salpeter equation. All MBPT calculations have been performed using the YAMBO code.[64] The comparison between DFT/TDDFT and MBPT has been previously reported for inorganic nanocrystals.[65−67] This is the first application to ZnO and ZnS clusters.

3. RESULTS AND DISCUSSION

We considered two families of unsaturated rod-shaped [0001] hexagonal nanocrystals with diameters $D1$ 0.5 nm and $D2$ 1 nm, respectively, and length L in the range ∼0.2 to 2.0 nm. The total number of dimers n forming the clusters $(ZnX)_n$ (X = O,S) ranges from 6 to 72. The initial ideal wurtzite structures and the final optimized geometries for selected examples of $D1$ and $D2$ nanocrystals are compared in Figures 1 and 2. Similar relaxed structures are found in all cases.

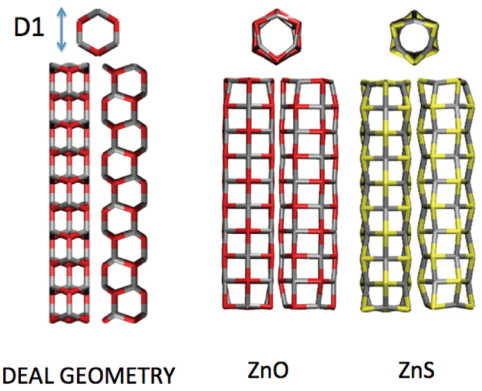

Figure 1. Orthogonal perspectives of an example of $D1$ nanocrystal ($D_1 \approx 0.5$ nm, length $L \approx 1.8$ nm, and n = 30). Left panel is the ideal prismatic wurtzite geometry and middle and right panels are the relaxed structures for ZnO and ZnS, respectively.

As clearly shown in Figures 1 and 2, after geometry optimization all of the systems considered maintain an almost unchanged hexagonal cross-section but loose completely the original wurtzite conformation along the [0001] direction. In particular, as a consequence of surface reconstruction, each cluster reaches a final configuration with inversion symmetry and thus has no net dipole moment. Interestingly, a very different behavior is observed for the two materials. ZnO wurtzite nanocrystals, both $D1$ and $D2$, transform into a

dx.doi.org/10.1021/jp209756z | J. Phys. Chem. C 2012, 116, 8741−8746

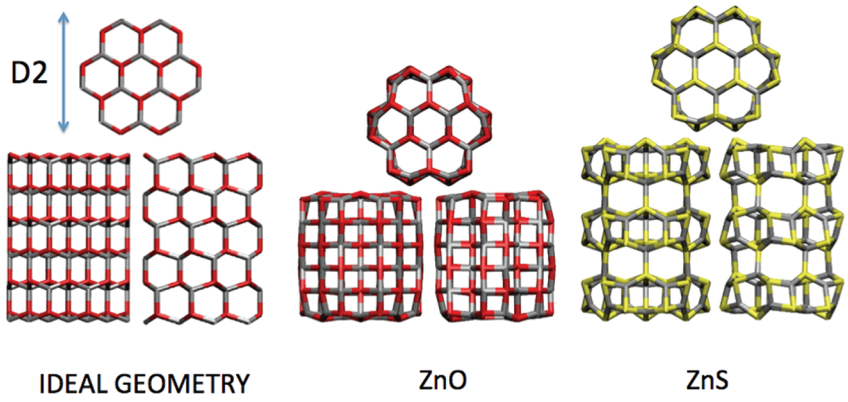

Figure 2. Orthogonal perspectives of an example of $D2$ nanocrystal ($D_2 \approx 1.0$ nm, length $L \approx 1.0$ nm, and $n = 72$). Left panel is the ideal prismatic wurtzite geometry and middle and right panels are the relaxed structures for ZnO and ZnS, respectively.

graphitic-like crystalline structure displaying a shortening along the [0001] direction as a direct consequence of the merging of Zn−O double layers. The planes of these graphitic systems, separated by an interlayer distance of ∼2.0 Å, are slightly distorted only at the top and bottom boundaries where side effects become dominant. These results, related to the polar (0001) surfaces in the ideal starting geometry, have been already reported in the literature[24,50,51] for ZnO nanostructures. In the case of ZnS, whereas small diameter $D1$ clusters undergo the same structural transformation to a graphitic phase as for the corresponding ZnO systems, $D2$ nanocrystals are found to reach a minimum energy configuration belonging to a completely different crystalline phase. Their geometry appears to be highly distorted along [0001] and can be viewed as composed of repeating units of $(ZnS)_{24}$ clusters placed at the average distance of ∼2.5 Å. The hexagonal cross-section together with the contemporary presence of four and six rings (Figure 2, right panel) reveals the occurrence of a zeolite BCT crystalline phase. The BCT phase has been predicted for large BCT particles on the basis of classical model potentials simulations.[41,45,46]

For each cluster, we computed the cohesive energy per dimer, E, as the difference between the total energy per dimer and the sum of the total energies of isolated atomic species ($Zn(^1S)$ and $O(^3P)$ or $S(^3P)$). This quantity, reported in Figure 3 as a function of n, gives a measure of the relative stability of the system: more negative values correspond to more stable clusters. For all families considered, we found that the stability increases with n. For both materials, as expected, $D2$ clusters

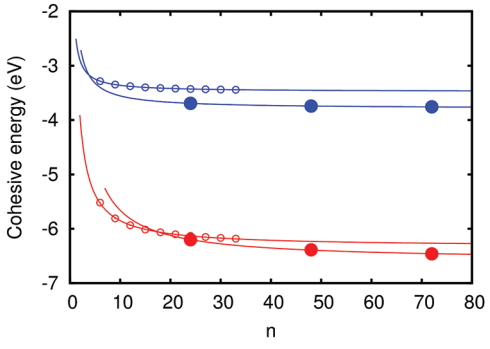

Figure 3. Cohesive energies as a function of n for ZnO (red) and ZnS (blue) nanocrystals with diameters $D1$ (small open circles) and $D2$ (big filled circles).

are more stable than $D1$. In addition, ZnO nanocrystals have larger cohesive energy than the corresponding ZnS systems, a result consistent with the larger cohesive energy measured for crystalline ZnO with respect to ZnS (−7.5 eV[68] vs −3.2[69]). The energy dependence on n can be explained by taking into account the energy cost associated with surface effects. This can be roughly estimated as $2\gamma N_d$, where N_d is the number of dangling bonds in the cluster and 2γ is an effective surface energy with units of energy per dangling bond. Accordingly, we can propose a simple model for the energy E

$$E = E^{bulk} + 2\gamma N_d/n \quad (2)$$

where E^{bulk} is the cohesive energy in the corresponding crystalline material. N_d can be explicitly expressed as a function of n for the $D1$ and $D2$ clusters as $N_d = (2n + 6)$ and $N_d = (n + 24)$, respectively. By using E^{bulk} and 2γ as adjustable parameters, we can fit the atomistic data by the above model (lines in Figure 3). The calculated E^{bulk} and 2γ, as well as the limiting value E^{∞}, are reported in Table 1. Because 2γ is an effective

Table 1. Parameters Obtained by Fitting the Computed Cohesive Energies through Equation 2 (see Figure 3)[a]

material	diameter	2γ	E^{bulk}	E^{∞}
ZnO	$D1$	0.8	−7.9	−6.3
	$D2$	0.4	−7.0	−6.6
ZnS	$D1$	0.2	−3.9	−3.5
	$D2$	0.1	−3.9	−3.8

[a] E^{bulk} and E^{∞} are given in eV/dimer and 2γ is expressed in units of eV/number of dangling bonds.

value (that includes, for example, the strain energy due to curvature), it is not expected to correspond to the surface energy of an infinite planar surface. In fact, for both materials, we found that the calculated values for $D1$ are two times those for $D2$; that is, γ is proportional to the curvature of the nanocrystal ($\gamma \approx 1/D$). Interestingly, we found that the effective surface energy of ZnO clusters is four times that of ZnS (for both $D1$ and $D2$). This difference is consistent with the larger $(10\bar{1}0)$ surface energy calculated for ZnO as compared with ZnS.[70]

Figure 4 displays, as a function of n, the fundamental gap computed via eq 1 (top), the optical gap as given by frequency space TDDFT (middle), and the exciton binding energy estimated through the difference between the fundamental gap and the optical gap (bottom). All of these quantities decrease at

dx.doi.org/10.1021/jp209756z | J. Phys. Chem. C 2012, 116, 8741−8746

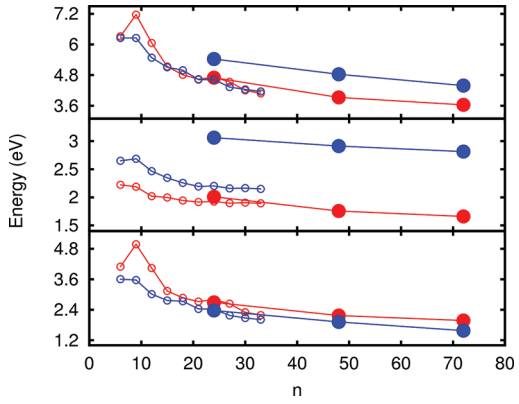

Figure 4. Fundamental gap (top), optical gap (middle), and exciton binding energy (bottom) as a function of n for ZnO (red) and ZnS (blue) nanocrystals with diameters $D1$ (small open circles) and $D2$ (big filled circles).

increasing n, as expected due to a reduction of quantum confinement. By comparing ZnO and ZnS, we found a general behavior that reflects the different structural transformations experienced by the two materials at increasing diameter. In the case of ZnO, the fundamental gap and the optical gap decrease almost monotonically when going from $D1$ to $D2$, which is related to the same structural transformation to a graphitic phase experienced by the two families. For ZnS, on the contrary, we found a strong discontinuity for these quantities as a consequence of the different crystalline phases, graphitic for $D1$ and BCT for $D2$. The exciton binding energy, estimated through the difference between the fundamental and optical gaps, results in the contrary insensitive to the crystalline rearrangement in ZnS, being much more affected by confinement effects. We found in all cases appreciable excitonic effects due to both quantum confinement and reduction of screening. The exciton binding energy values for ZnO nanocrystals are always larger than those for the ZnS counterparts, which agrees with the differences measured for the same quantity in the bulk materials (about 60 meV vs 40 meV).

To estimate quantitatively the differences of the electronic properties between the BCT and wurtzite phases in ZnS nanocrystals, we additionally considered an intermediate-size $D2$ model particle (n = 48), saturated according to the prescriptions given in ref 49. In detail, we saturated the cluster by dissociating six H_2X molecules, adsorbing H^+ and HX^- ions on the polar X and Zn surfaces, respectively. For completeness, we considered also the corresponding model for ZnO. The saturated model particles, for both ZnS and ZnO, preserve the wurtzite crystalline phase according to previous results.[49] We found that the saturated wurtzite and unsaturated graphitic ZnO particles have similar well-opened energy gaps (~1.7 eV) without surface intraband-gap states. The spatial distribution of the frontier orbitals is similar, and the LUMO state, in particular, is delocalized in the entire cluster for both saturated and unsaturated models. The main effect of saturation is to upshift rigidly the electronic levels (by ~0.3 eV). In the case of the saturated ZnS wurtzite particle, a major energy upshift is observed only for the HOMO state so that the HOMO−LUMO gap for the unsaturated BCT particle (2.9 eV) is much larger than that in the wurtzite case (2.3 eV). This result further confirms that the discontinuity in the size-dependent optoelectronic properties of ZnS $D1$ and $D2$ nanocrystals is related to the occurrence of a BCT phase.

4. MANY-BODY CALCULATIONS AND PHOTOABSORPTION SPECTRA

From the methodological point of view, we additionally made use of MBPT to validate the DFT/TDDFT results. The fundamental gaps of 6.32 and 6.26 eV for $(ZnO)_6$ and $(ZnS)_6$ calculated via eq 1 can be compared with the corresponding G_0W_0 results of 6.9 and 6.6 eV. The agreement is reasonable, taking into account the fact that the two methods usually give differences of some tenths of electronvolts for clusters.[65−67] The absorption spectra of $(ZnO)_6$ and $(ZnS)_6$ from BSE and TDDFT calculations are reported in Figure 5. The spectra

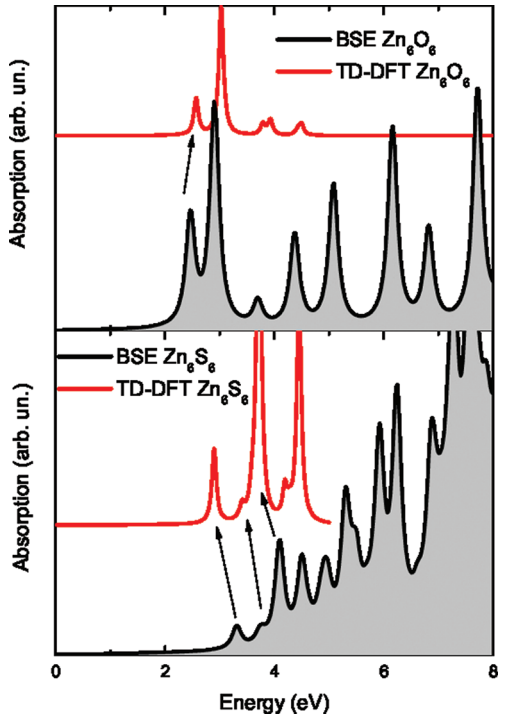

Figure 5. Comparison between the absorption spectra of $(ZnO)_6$ (top) and $(ZnS)_6$ (bottom) as obtained from BSE and TDDFT. The BSE spectrum for $(ZnS)_6$ is in good quantitative agreement with the B3LYP spectrum reported in ref 47.

display similar shapes, indicating that optical transitions are described in the same way by the two methods, the very accurate GW+BSE method and the less computationally demanding TDDFT approach; the small shift is due to the inclusion of the GW gap opening in the MBPT calculations. Note that for inorganic compounds this is not always the case because there are several cases reported in the literature for which TDDFT does not take fully into account the interactions involved in optical transitions and gives therefore only a qualitative picture.[65−67] The application of TDDFT to the whole set of nanocrystals considered as done in the previous section is therefore justified. From the analysis of excitonic energies and contributions, we find that for both materials the first two transitions (HOMO→LUMO and HOMO-1→LUMO) are optically dark. The first optically active transition, at 2.57 eV with oscillator strength 0.030 for $(ZnO)_6$ and 2.90 eV with oscillator strength 0.016 for $(ZnS)_6$, is given by HOMO-2→LUMO states and is polarized along the [0001] axis of the cluster. The exciton binding energies, calculated from MBPT are 3.6 and 3.4 eV for $(ZnO)_6$ and $(ZnS)_6$, respectively, which compare fairly well with the estimates of

dx.doi.org/10.1021/jp209756z | J. Phys. Chem. C 2012, 116, 8741−8746

3.75 and 3.36 eV obtained through the difference between the fundamental DFT gap and the TDDFT optical gap. The good agreement validates the application of TDDFT to the whole set of nanocrystals considered, for which GW and BSE calculations are prohibitively expensive.

Figure 6 displays the complete absorption spectra of ZnO and ZnS *D*1 nanocrystals as obtained through the real-time

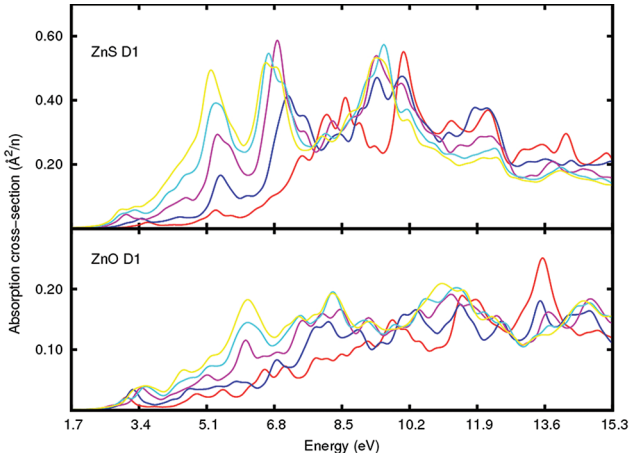

Figure 6. Absorption cross sections of $(ZnO)_n$ (bottom) and $(ZnS)_n$ (top) *D*1 nanocrystals (red, blue, violet, cyan, and yellow correspond to n = 6, 12, 18, 24, and 30, respectively).

real-space TDDFT implementation of the OCTOPUS code. To ease the comparison, we normalized the spectra to the total number of dimers n. At increasing sizes, both compounds display a continuous red shift of the main peaks in the absorption spectrum. This behavior was expected as a consequence of the continuous decrease in the optical gap already observed from the frequency space TDDFT results (cf. Figure 4). In the case of ZnO *D*1 nanocrystals our results are consistent with those reported in ref 35 for saturated model particles in the low-energy range up to 4.0 eV. At fixed n, the absorption cross sections are always found to be larger for ZnS clusters.

5. CONCLUSIONS

We reported a systematic theoretical study of the structural and size-dependent optoelectronic properties of unsaturated ZnO and ZnS nanoclusters with hexagonal prism structure. We used DFT in the gradient-corrected approximation to perform structural relaxations. The fundamental gap and the optical gap have been computed in the framework of the ΔSCF scheme and TDDFT, respectively. The difference between the fundamental gap and the optical gap enabled a rough estimate of the excitonic effects occurring in the systems studied. We compared our results for two distinct families of nanocrystals, *D*1 and *D*2, with different surface-to-volume ratios, diameters of about 0.5 and 1.0 nm, respectively, and increasing length along the [0001] direction from 0.2 to 2.0 nm for *D*1 and from 0.2 to 1.0 nm for *D*2. We found in all cases significant structural rearrangements as a consequence of surface effects. Ground-state structural relaxations reveal that ZnO systems transform from wurtzite to a graphitic phase. ZnS *D*2 nanocrystals on the contrary, while preserving the hexagonal cross-section, are highly distorted along the [0001] direction and transform to a zeolite BCT crystalline phase. These different crystal structure rearrangements are reflected in very different energetic, electronic, and optical properties. To correlate the morphological and optoelectronic properties, we additionally considered models of saturated clusters preserving the wurtzite phase. We found that the properties of ZnO graphitic and wurtzite clusters are relatively similar, whereas those of ZnS BCT particles differ sizeably from those of the corresponding wurtzite-like clusters. From the methodological side, we made use of MBPT for the smallest clusters of the two materials. We found good agreement between DFT/TDDFT results and MBPT methods. In particular, TDDFT and BSE give the same description, confirming the absence of charge transfer phenomena in these nanostructures and the possibility of applying TDDFT to nanosystems that cannot be afforded by MBPT methods.

■ ASSOCIATED CONTENT

Ⓢ Supporting Information

Additional details of the calculations and references. This material is available free of charge via the Internet at http://pubs.acs.org/.

■ AUTHOR INFORMATION

Corresponding Author

*E-mail: giuliano.malloci@dsf.unica.it; alessandro.mattoni@dsf.unica.it. Phone: +39 070 6754843. Fax: +39 070 510171.

Notes

The authors declare no competing financial interest.

■ ACKNOWLEDGMENTS

This work has been funded by the Italian Institute of Technology (IIT) under Project SEED "POLYPHEMO" and Regione Autonoma della Sardegna under L.R.7/2007. We acknowledge financial support from Spanish MEC (FIS2011-65702-C02-01), ACI-Promociona (ACI2009-1036), Grupos Consolidados UPV/EHU del Gobierno Vasco (IT-319-07), and the European Research Council Advanced Grant DYNamo (ERC-2010-AdG -proposal no. 267374). We acknowledge computational support by IIT Platform "Computation", CYBERSAR (Cagliari), CINECA (Bologna), CASPUR (Rome), National Supercomputing Center (Barcelona), "Red Espanola de Supercomputacion", and SGIker ARINA (UPV/EHU). We are also grateful to Matteo Dessalvi for technical support.

■ REFERENCES

(1) Kroto, H. W.; Heath, J. R.; Obrien, S. C.; Curl, R. F.; Smalley, R. E. *Nature* **1985**, *318*, 162−163.
(2) Iijima, S. *Nature* **1991**, *354*, 56−58.
(3) Fang, X.; Bando, Y.; Gautam, U. K.; Zhai, T.; Zeng, H.; Xu, X.; Liao, M.; Golberg, D. *Crit. Rev. Solid State Mater. Sci.* **2009**, *34*, 190−223.
(4) Pan, Z. W.; Dai, Z. R.; Wang, Z. L. *Science* **2001**, *291*, 1947−1949.
(5) Huang, M. H.; Mao, S.; Feick, H.; Yan, H.; Wu, Y.; Kind, H.; Weber, E.; Russo, R.; Yang, P. *Science* **2001**, *292*, 1897−1899.
(6) Ma, C.; Moore, D.; Li, J.; Wang, Z. L. *Adv. Mater.* **2003**, *15*, 228−231.
(7) Tian, Z. R.; Voigt, J. A.; Liu, J.; McKenzie, B.; McDermott, M. J.; Rodriguez, M. A.; Konishi, H.; Xu, H. *Nat. Mater.* **2003**, *2*, 821−826.
(8) Kong, X. Y.; Wang, Z. L. *Nano Lett.* **2003**, *3*, 1625−1631.
(9) Gao, P. X.; Ding, Y.; Mai, W.; Hughes, W. L.; Lao, C.; Wang, Z. L. *Science* **2005**, *309*, 1700−1704.
(10) Fang, X.; Zhai, T.; Gautam, U. K.; Li, L.; Wu, L.; Y., B.; Golberg, D. *Prog. Mater. Sci.* **2011**, *56*, 175−287.

(11) Yan, J.; Fang, X.; Zhang, L.; Bando, Y.; Gautam, U. K.; Dierre, B.; Sekiguchi, T.; Golberg, D. *Nano Lett.* **2008**, *8*, 2794−2799.
(12) Yu, X.; Ji, H.; Wang, H.; Sun, J.; Du, X. *Nanoscale Res. Lett.* **2010**, *5*, 644−648.
(13) Law, M.; Greene, L. E.; Johnson, J. C.; Saykally, R.; Yang, P. *Nat. Mater.* **2005**, *4*, 455−459.
(14) Martinson, A. B. F.; Elam, J. W.; Hupp, J. T.; Pellin, M. J. *Nano Lett.* **2007**, *7*, 2183−2187.
(15) Han, J.; Fan, F.; Xu, C.; Lin, S.; Wei, M.; Duan, X.; Wang, Z. L. *Nanotechnology* **2010**, *21*, 405203.
(16) Ko, S. H.; Lee, D.; Kang, H. W.; Nam, K. H.; Yeo, J. Y.; Hong, S. J.; Grigoropoulos, C. P.; Sung, H. J. *Nano Lett.* **2011**, *11*, 666−671.
(17) Vogel, R.; Hoyer, P.; Weller, H. *J. Phys. Chem.* **1994**, *98*, 3183−3188.
(18) Leschkies, K. S.; Divakar, R.; Basu, J.; Enache-Pommer, E.; Boercker, J. E.; Carter, C. B.; Kortshagen, U. R.; Norris, D. J.; Aydil, E. S. *Nano Lett.* **2007**, *7*, 1793−1798.
(19) Kamat, P. V. *J. Phys. Chem. C* **2008**, *112*, 18737−18753.
(20) Behrman, E. C.; Foehrweiser, R. K.; Myers, J. R.; French, B. R.; Zandler, M. E. *Phys. Rev. A* **1994**, *49*, R1543−R1546.
(21) Lü, X.; Xu, X.; Wang, N.; Zhang, Q.; Ehara, M.; Nakatsuji, H. *Chem. Phys. Lett.* **1998**, *291*, 445−452.
(22) Matxain, J. M.; Mercero, J. M.; Ugalde, J. M. *J. Am. Chem. Soc.* **2003**, *125*, 9494−9499.
(23) Jain, A.; Kumar, V.; Kawazoe, Y. *Comput. Mater. Sci.* **2006**, *36*, 258−262.
(24) Li, C.; Guo, W.; Kong, Y.; Gao, H. *Appl. Phys. Lett.* **2007**, *90*, 223102.
(25) Li, C.; Guo, W.; Kong, Y.; Gao, H. *Phys. Rev. B* **2007**, *76*, 035322.
(26) Reber, A. C.; Khanna, S. N.; Hunjan, J. S.; Beltran, M. R. *Eur. Phys. J. D* **2007**, *43*, 221−224.
(27) Zhao, M.; Xia, Y.; Tan, Z.; Liu, X.; Mei, L. *Phys. Lett. A* **2007**, *372*, 39−43.
(28) Wang, B.; Nagase, S.; Zhao, J.; Wang, G. *J. Phys. Chem. C* **2007**, *111*, 4956−4963.
(29) Wen, B.; Melnik, R. *Chem. Phys. Lett.* **2008**, *466*, 84−87.
(30) Wang, B.; Wang, X.; Chen, G.; Nagase, S.; Zhao, J. *J. Chem. Phys.* **2008**, *128*, 144710.
(31) Cheng, X.; Li, F.; Zhao, Y. *J. Mol. Struct.* **2009**, *894*, 121−127.
(32) Wang, B.; Wang, X.; Zhao, J. *J. Phys. Chem. C* **2010**, *114*, 5741−5744.
(33) Botello-Méndez, A. R.; López-Urías, F.; Terrones, M.; Terrones, H. *Chem. Phys. Lett.* **2010**, *492*, 82−88.
(34) Schoenhalz, A. L.; Arantes, J. T.; Fazzio, A.; Dalpian, G. M. *J. Phys. Chem. C* **2010**, *114*, 18293.
(35) De Angelis, F.; Armelao, L. *Phys. Chem. Chem. Phys.* **2011**, *13*, 467−475.
(36) Matxain, J. M.; Fowler, J. E.; Ugalde, J. M. *Phys. Rev. A* **2000**, *61*, 053201.
(37) Matxain, J. M.; Irigoras, A.; Fowler, J. E.; Ugalde, J. M. *Phys. Rev. A* **2001**, *64*, 013201.
(38) Spanó, E.; Hamad, S.; Catlow, C. R. A. *J. Phys. Chem. B* **2003**, *107*, 10337.
(39) Pal, S.; Goswami, B.; Sarkar, P. *J. Chem. Phys.* **2005**, *123*, 044311.
(40) Hamad, S.; Catlow, C. R. A.; Spanó, E.; Matxain, J. M.; Ugalde, J. M. *J. Phys. Chem. B* **2005**, *109*, 2703−2709.
(41) Hamad, S.; Catlow, C. R. A. *J. Cryst. Growth* **2006**, *294*, 2−8.
(42) Matxain, J. M.; Eriksson, L. A.; Mercero, J. M.; Ugalde, J. M.; Spano, E.; Hamad, S.; Catlow, C. R. A. *Nanotechnology* **2006**, *17*, 4100−4105.
(43) Zhang, X.; Zhao, M.; He, T.; Li, W.; Lin, X.; Wang, Z.; Xi, Z.; Liu, X.; Xia, Y. *Solid State Commun.* **2008**, *147*, 165−168.
(44) Pal, S.; Sharma, R.; Goswami, B.; Sarkar, P.; Bhattacharyya, S. P. *J. Chem. Phys.* **2009**, *130*, 214703.
(45) Hamad, S.; Woodley, S. M.; Catlow, C. R. A. *Mol. Simul.* **2009**, *35*, 1015−1032.
(46) Catlow, C. R. A.; Bromley, S. T.; Hamad, S.; Mora-Fonz, M.; Sokol, A. A.; Woodley, S. M. *Phys. Chem. Chem. Phys.* **2010**, *12*, 786−811.
(47) Zwijnenburg, M. A.; Sousa, C.; Illas, F.; Bromley, S. T. *J. Chem. Phys.* **2011**, *134*, 064511.
(48) Zhang, S.; Ma, J. *J. Phys. Chem. C* **2011**, *115*, 4466−4475.
(49) Azpiroz, J. M.; Mosconi, E.; De Angelis, F. *J. Phys. Chem. C* **2011**, *115*, 25219−25226.
(50) Zhang, L.; Huang, H. *Appl. Phys. Lett.* **2006**, *89*, 183111(1−3).
(51) Zhang, L.; Huang, H. *Appl. Phys. Lett.* **2007**, *90*, 023115(1−3).
(52) Jones, R. O.; Gunnarsson, O. *Rev. Mod. Phys.* **1989**, *61*, 689−746.
(53) Onida, G.; Reining, L.; Rubio, A. *Rev. Mod. Phys.* **2002**, *74*, 601.
(54) Marques, M. A. L.; Gross, E. K. U. *Annu. Rev. Phys. Chem.* **2004**, *55*, 3425−3433.
(55) Becke, A. D. *J. Chem. Phys.* **1988**, *88*, 1053.
(56) Perdew, J. P. *Phys. Rev. B* **1986**, *33*, 8822−8824.
(57) Decremps, F.; Datchi, F.; Saitta, A. M.; Polian, A.; Pascarelli, S.; di Cicco, A.; Itié, J. P.; Baudelet, F. *Phys. Rev. B* **2003**, *68*, 104101.
(58) Bauernschmitt, R.; Ahlrichs, R. *Chem. Phys. Lett.* **1996**, *256*, 454−464.
(59) Yabana, K.; Bertsch, G. F. *Int. J. Quantum Chem.* **1999**, *75*, 55−66.
(60) TURBOMOLE V6.2 2010, a development of University of Karlsruhe and Forschungszentrum Karlsruhe GmbH, 1989−2007, TURBOMOLE GmbH, since 2007. http://www.turbomole.com; accessed Oct 3, 2011.
(61) Marques, M. A. L.; Castro, A.; Bertsch, G. F.; Rubio, A. *Comput. Phys. Commun.* **2003**, *151*, 60−78.
(62) Hedin, L. *Phys. Rev.* **1965**, *139*, 796−823.
(63) Godby, R. W.; Schlüter, M.; Sham, L. J. *Phys. Rev. B* **1988**, *37*, 10159−10175.
(64) Marini, A.; Hogan, C.; Grüning, M.; Varsano, D. *Comput. Phys. Commun.* **2009**, *180*, 1392−1403.
(65) Tiago, M. L.; Chelikowsky, J. R. *Phys. Rev. B* **2006**, *73*, 205334.
(66) Lopez del Puerto, M.; Tiago, M. L.; Chelikowsky, J. R. *Phys. Rev. B* **2008**, *77*, 045404.
(67) Chiodo, L.; Salazar, M.; Romero, A. H.; Laricchia, S.; Sala, F. D.; Rubio, A. *J. Chem. Phys.* **2011**, *135*, 244704.
(68) Özgür, Ü.; Alivov, Y. I.; Liu, C.; Teke, A.; Reshchikov, M. A.; Doğan, S.; Avrutin, V.; Cho, S.-J.; Morkoç, H. *J. Appl. Phys.* **2005**, *98*, 041301−103.
(69) Benkabou, F.; Aourag, H.; Certier, M. *Mater. Chem. Phys.* **2000**, *66*, 10−16.
(70) Na, S.-H.; Park, C.-H. *J. Korean Phys. Soc.* **2010**, *56*, 498−502.